INTERNATIONAL SOCIETY FOR SOIL MECHANICS AND GEOTECHNICAL ENGINEERING

Relation between liquefaction resistance and shear modulus of crushable volcanic soils

Mohammad Bagher Asadi[1], *Rolando* Orense[2#], and *Mohammad Sadeq Asadi*[1]

[1]*Geotechnical Engineer, Jacobs Ltd, Auckland New Zealand*
[2]*Department of Civil & Environmental Engineering, University of Auckland, New Zealand*
[#]*Corresponding author: r.orense@auckland.ac.nz*

ABSTRACT

Pumice-rich soils originating from volcanic eruptions are deposited in various parts of the world, such as in the central region of North Island, NZ. The pumice sand components of these natural pumiceous (NP) soils are known to be crushable and lightweight, resulting in a significant difference in their cyclic resistance ratio (CRR) and small-strain shear modulus (G_{max}) when compared to hard-grained (quartz) sands. In this paper, the results of a number of cyclic triaxial and bender element tests performed on reconstituted specimens of three types of NP sands having different pumice contents (PC), as well as on quartz-type Toyoura sand specimens, are discussed. Then, the concept of modified cyclic yield strain, $\varepsilon_{ay,m}$, which relates the CRR of the specimen to its G_{max}, is used. The results indicate that $\varepsilon_{ay,m}$ appears to be dependent only on the soil type, and independent of the confining pressure applied and the relative density of the specimen. All NP sand specimens show higher $\varepsilon_{ay,m}$ when compared to Toyoura sand because of their higher CRR and lower G_{max}, with values of $\varepsilon_{ay,m}$ increasing as the PC of the specimen increases. Based on the results obtained, an empirical chart is developed to estimate the CRR of NP sands from their shear wave velocity (V_s) values under field conditions.

Keywords: Pumiceous sand; liquefaction resistance; small-strain shear modulus; volcanic soils.

1. Introduction

Pumice-rich deposits are found in several areas in the central region of the North Island, New Zealand, mainly as a result of volcanic eruptions centred in the Taupo Volcanic Zone. The pumice-rich pyroclastic flows from these eruptions were transported airborne and then deposited in wide areas in the Waikato Basin through erosion and river transport. In the process, the pumice sand particles were mixed with other soils in the area; the deposits are herein referred to as natural pumiceous (NP) sands. The pumice sand particles are characterised by their crushability and compressibility (Orense et al. 2012). Hence, questions are raised as to whether existing empirical correlations, derived from ordinary (hard-grained) sands, apply to NP sands.

Studies conducted by the authors indicate that the liquefaction resistance (or cyclic resistance ratio, CRR) of reconstituted NP sands is much higher than those of ordinary sands under similar density states. This is presumably due to the very irregular and complex surface textures of the pumice sand grains, which cause the specimens to form a stable condition during undrained cyclic shearing and be more resistant to liquefaction (Asadi et al. 2018). Moreover, test results showed that the small-strain shear modulus, G_{max}, of NP sands is considerably lower than that of Toyoura sand over a wide range of effective confining pressures, σ'_c, and post-consolidation void ratios, e (Asadi et al. 2020). The values of CRR and G_{max} are dependent on the pumice content (PC) of the specimens, with specimens containing more pumice sands (higher PC) having higher CRR and lower G_{max}.

In this paper, the undrained cyclic response and small-strain dynamic characteristics of NP sands are first summarised, with emphasis on the effect of the PC of the specimens on their CRR and G_{max}. Next, an attempt is made to formulate a relationship between the two parameters, from which a relation between the CRR and G_{max} of reconstituted specimens is developed taking into account field conditions.

2. Materials and Testing Programme

Disturbed NP sands were obtained as bulk samples from test pits at NP1, NP2, NP3, and NP4 sites within the Waikato Basin. Fig. 1 shows the location of the sites. Sites NP1 and NP2 were located in Hamilton City while site NP3 was near Rangiriri Town and site NP4 was in Huntly. The NP materials were sourced at depths of 1.5 m, 2.0 m, 4.5 m, and 5.5 m, respectively, for NP1, NP2, NP3, and NP4 sites. These depths were chosen because borehole logs showed the presence of pumice-rich layers at these depths. For comparison purposes, Toyoura sand, a well-known hard-grained, sub-angular material, was also tested in the laboratory.

The index properties of the materials tested are summarised in Table 1 while their particle size distribution (PSD) curves are shown in Fig. 2. The pumice contents indicated in the table for each NP sand were obtained using the modified maximum dry density (MDD) method proposed by Asadi et al. (2019), which considers the breakage potential of the pumice sand components within the pumiceous soil matrix.
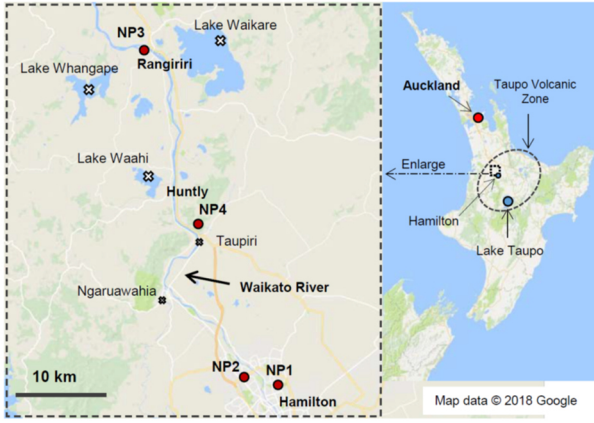
Figure 1. Locations where the natural pumiceous materials were sampled (map data © 2018 Google).

Table 1. Index properties of the materials tested.

Material	Spec. gravity	Max. dry density (g/cm³)	Min. dry density (g/cm³)	Pumice content (%)
NP1	2.53	1.54	1.27	21
NP2	2.50	1.38	1.07	32
NP3	2.54	1.24	0.93	39
NP4	2.48	1.27	0.97	49
Toyoura	2.66	1.64	1.40	-

Fig. 3 shows the images of the NP1 and NP3 sand particles taken by scanning electron microscope (SEM). It is clear that the pumice sand particles have a unique appearance when compared to the hard-grained sand components of the NP sands.

The reconstituted specimens for the triaxial tests were prepared by the moist tamping method; this method was chosen to form uniform test specimens and to avoid particle segregation (due to the low solid density of the pumice particles compared to the hard-grained constituents and the presence of fine particles within the NP samples).

The target size of the triaxial specimen was 63 mm in diameter and 126 mm high. Prior to preparing the sample, the soil materials were mixed with water to form moist soil samples with a water content of around 20–30%. The triaxial specimen was prepared in a sample split mould on top of the base of the triaxial apparatus in order to achieve a specified target relative density after consolidation, D_{rc}. To ensure uniform density throughout the specimen, each specimen was prepared in five layers in the sample split mould using a procedure similar to the under-compaction method proposed by Ladd (1978). For each target density, a pre-weighed quantity was used for each layer that was then compacted by gentle tapping using a tamper (with a diameter of 25 mm) until the required thickness of each layer was achieved.

After reaching the target specimen height (corresponding to a target D_{rc}), a groove was carefully made on top of the specimen along the same orientation as the bender element (BE) on the pedestal. The top cap, with another BE installed, was placed on top of the specimen to fit the BE into the groove perfectly. Next, the sample was saturated by the application of back
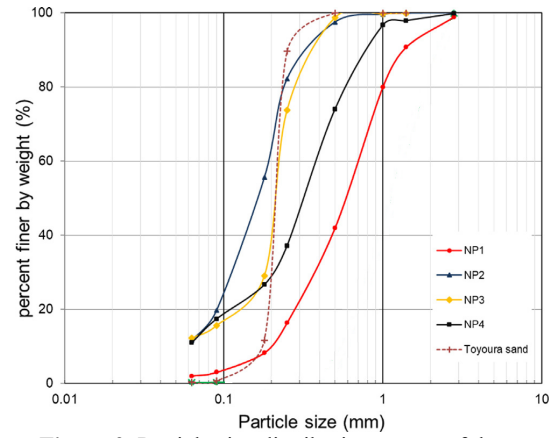

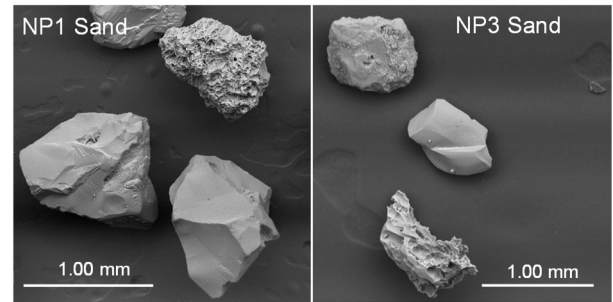**Figure 2.** Particle size distribution curves of the materials tested.

Figure 3. Typical SEM images of the NP sands tested. The pumice sand components are characterised by their irregular surface texture and the presence of surface voids.

pressure in stages, and back pressure of 500-600 kPa was required to achieve a B-value > 0.95.

During the consolidation phase, the cell pressure was increased to the desired level. Firstly, the BE test was conducted to measure the shear wave velocity, V_s, of the specimen. Several BE tests at different effective confining pressures, σ'_c, were conducted on single specimens. Next, cyclic loading was applied to the specimen until liquefaction occurred. Here, liquefaction was defined as the condition when the specimen reached a double amplitude axial strain $\varepsilon_{DA}=5\%$.

3. Results and discussions

3.1. Small-strain shear modulus, G_{max}

A number of BE tests with different initial void ratios, e_i (loose to medium dense) were conducted on the reconstituted soil specimens to establish their G_{max} - σ'_c plot under similar post-consolidation void ratio, e, and different levels of σ'_c. The values of e corresponding to approximately $D_{rc} \approx 55\%$ over the applied levels of σ'_c were obtained from the results to establish the G_{max} - σ'_c relations (with constant e) for all tested sands, and these are illustrated in Fig. 4. As shown in the figure, the value of G_{max} increases with the increase in σ'_c, which is consistent with the observations made on other granular materials by various researchers. It can be seen that the G_{max} of NP sands is considerably lower than that of Toyoura sand under similar D_{rc}. Furthermore, the results indicate that the G_{max} dependency of NP sands on σ'_c is more pronounced compared to Toyoura sand. For example, as evident from the plot, the slopes of the G_{max}
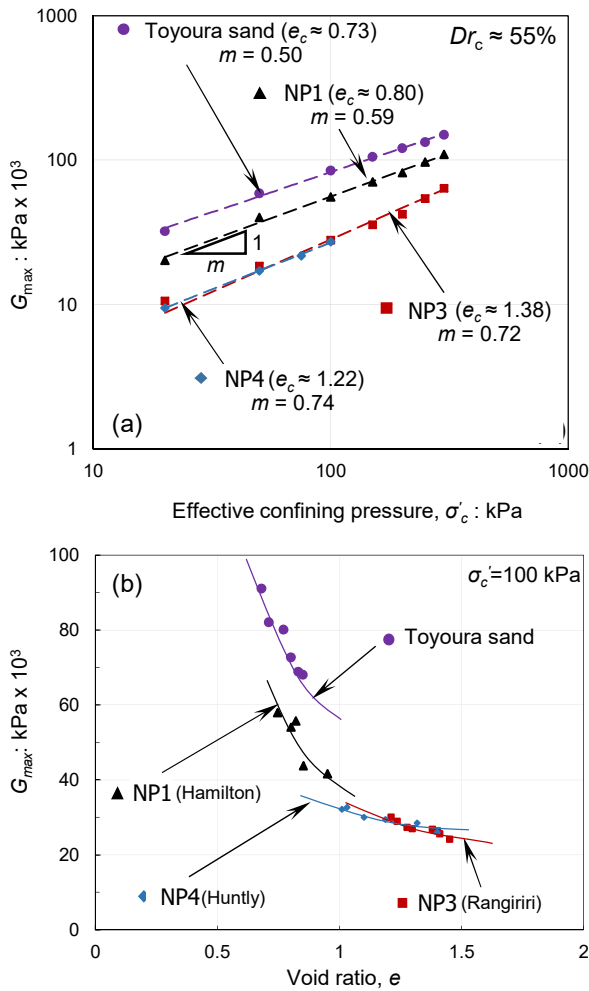
Figure 4. Plots showing the effect of (a) confining pressure, σ'_c; and (b) post-consolidation void ratio, e, on the G_{max} of the tested materials.

- σ'_c relation (i.e., m–value, in log-log scale) for NP3, NP4, and NP1 specimens are 0.72, 0.74, and 0.59, respectively, while that for Toyoura sand is 0.50. Note that the test result for Toyoura sand is consistent with the results reported in the literature. Moreover, the observed behaviour of NP sands at a particular value of e is similar to those of other volcanic soils investigated in literature (e.g., Touhoro, Tomikawa and Shirasu), that showed lower G_{max} and stronger influence of σ'_c on the G_{max}, i.e., higher m-value (Miura et al. 2003; Sahaphol & Miura 2005).

The fact that the G_{max} dependency on σ'_c for NP sands was more pronounced compared to Toyoura sand may be due to the irregular surface texture of the pumice sand components within the NP sands, with their high angularity and elongated features, as well as their compressibility (as manifested by particle crushing during the tests); these lead to better particle contacts in the NP sand specimens with the increase in σ'_c.

The G_{max} - e relations for the NP sands and Toyoura sand were also investigated over a wide range of e at different levels of σ'_c. Fig. 4(b) compares the G_{max} - e relations of the tested sand specimens at similar $\sigma'_c = 100$ kPa. It can be seen from the plot that the G_{max} - e dependency of NP3 and NP4 sands is significantly different from NP1 sand. For example, in the case of NP1, e significantly affects the G_{max} value and roughly

behaves similarly to the hard-grained Toyoura sand; however, the results for NP3 and NP4 sands show that their G_{max} values are less dependent on the void ratio variations. Note that the observed trend for Toyoura sand obtained in this research shows a similar G_{max} - e curve as that reported by Kokusho (1980). This observation on NP sands can be explained by considering the high void ratio range ($e_{max} - e_{min}$) and high particle crushing manifestation for NP3 and NP4 sands (with their higher pumice contents) when compared to NP1 sand and Toyoura sand.

3.2. Liquefaction resistance ratio, *CRR*

Fig. 5 illustrates typical undrained cyclic responses of dense (D_r=80%) NP sands and Toyoura sand in terms of the generation of double amplitude axial strain (ε_{DA}) and excess pore water pressure ratio, r_u, with respect to the normalised number of cycles (i.e., the number of cycles, N_c, was normalised by the N_c required to reach ε_{DA}=5%. It can be seen from the figure that the trends of ε_{DA} and r_u developments for NP sands, subjected to different levels of cyclic stress ratios, *CSR*, are considerably different from those of Toyoura sand. For Toyoura sand, negligible strains develop on the specimens under the application of a significant number of cyclic loading. However, as soon as the specimens reach the instability point (i.e., phase transformation), the rate of strain development increases dramatically. Toyoura sand specimens underwent an immediate increase in r_u as soon as the specimens were subjected to cyclic loading. This is followed by a gradual increase in r_u until the instability point is reached. From then onwards, an immediate increase in r_u is observed.

On the other hand, dense NP sand specimens undergo an initial deformation with the first cycle of loading, accompanied by high r_u development. In the subsequent loading cycles, the strain development gradually increases almost linearly until ε_{DA}=5%. In terms of the excess pore water pressure, there is an immediate increase in value, with r_u reaching 0.8 during the first quarter of cyclic loading; this is followed by a gradual increase in the second quarter of cyclic loading until r_u =0.95 is reached.

Thus, compared to Toyoura sand, NP sands generally show a different undrained cyclic response in terms of axial strain and pore water pressure development. NP sands undergo a gradual but steady deformation from the beginning of the cyclic loading until the occurrence of liquefaction. With the application of the initial cycle of loading, NP sands show a very contractive behaviour as a result of particle crushing; under high r_u values, they show a very strong dilative behaviour. Dense NP sands are capable of being subjected to a significant number of cyclic loading under high r_u, due to the stable skeleton formed as the cyclic shearing progresses.

Although not shown here, loose NP sand specimens also showed a similar response; however, dense NP sand specimens undergo more particle crushing during cyclic loading than loose specimens.

The liquefaction resistance curves for the materials tested are shown in Fig. 6, relating the number of cycles required to attain ε_{DA}=5% for the specified *CSR*. It is clear
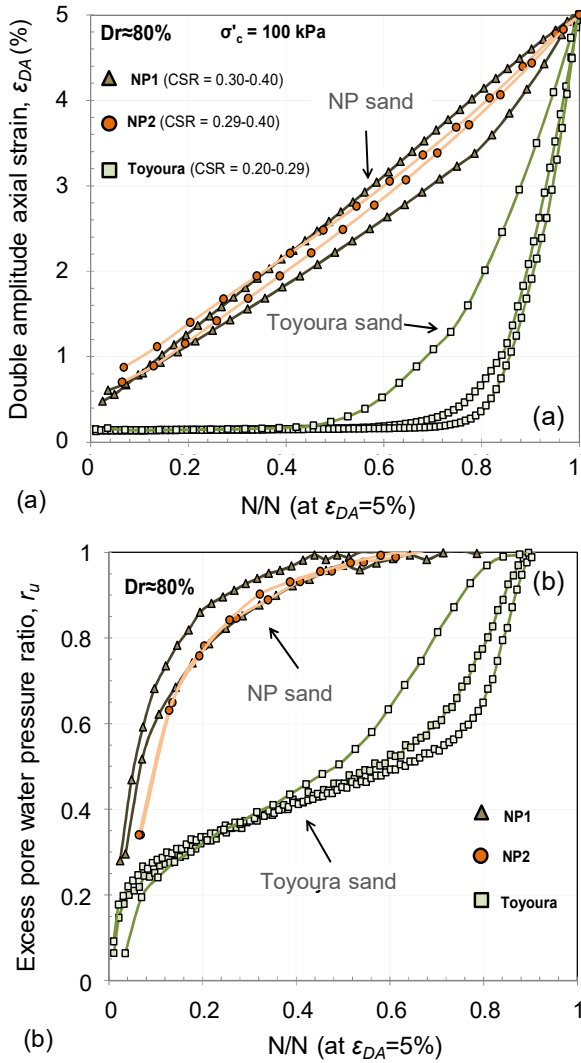
Figure 5. Comparison of the development of (a) double amplitude axial strain, ε_{DA}; and (b) excess pore water pressure ratio, r_u, between Toyoura sand and NP sands.

that the liquefaction resistance of NP sands increases with increasing relative density, consistent with the observation reported on hard-grained sands, such as Toyoura sand. Moreover, for similar density, NP sands are more resistant to liquefaction compared to Toyoura sand. This can be attributed to better soil re-structuration in NP sand specimens (from particle crushing and
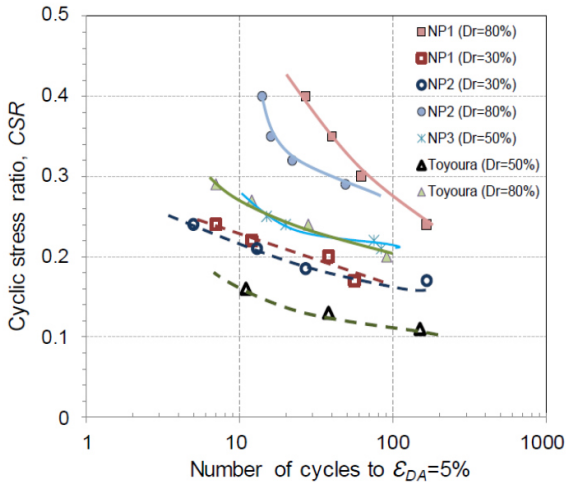

Figure 6. Liquefaction resistance curves of the materials tested.

particle re-arrangement) as the cyclic loading progresses, providing a better contact/engagement between the particles, that leads to their higher *CRR* values.

3.3. *CRR*-G_{max} relation

As explained above, the G_{max} values of NP sands are considerably lower than those of normal sands. Thus, the higher deformability of the pumice sand components during the initial stages of the cyclic loading (which leads to faster ε_{DA} and r_u development) can be linked to their lower G_{max} values. On the other hand, Toyoura sand, with its higher G_{max}, shows negligible deformation during the initial stages of cyclic loading. Although NP sands have faster ε_{DA} and r_u development during the initial stages of cyclic loading when compared with Toyoura sand, they have higher liquefaction resistance.

Fig. 7 illustrates the relations between *CRR* and G_{max} for the investigated NP sands with different *PC*, as well as those of Toyoura sand, under σ'_c=100 kPa. It can be seen that the NP sands have different *CRR* - G_{max} trends depending on their *PC*. Furthermore, the NP sands have substantially different *CRR* - G_{max} relations when compared with Toyoura sand, with NP sands having higher *PC* showing a steeper *CRR* - G_{max} plot. In other words, the *CRR*/G_{max} ratio for Toyoura sand is considerably lower when compared to NP sands. These results suggest that the *CRR*/G_{max} ratio can be used to distinguish the NP sands with different *PC* from ordinary sands (e.g. Toyoura sand).
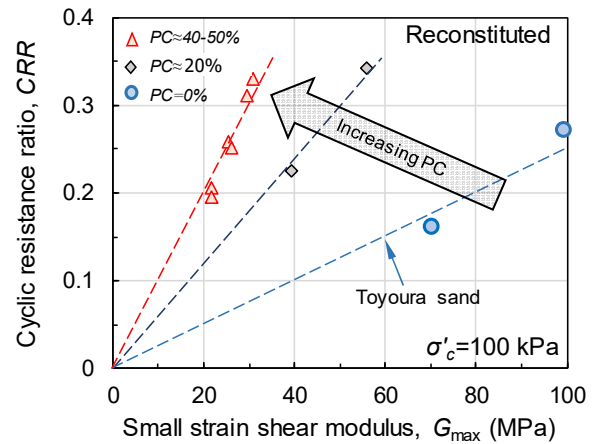

Figure 7. Relationship between *CRR* and G_{max} of the tested sands as a function of pumice content.

3.4. Cyclic yield strain concept

Amoly et al. (2016) reported that the *CRR*/G_{max} ratio could be related to a reference strain index, denoted as cyclic yield strain, ε_{ay}, an important parameter that can be used as a benchmark level of strain to differentiate liquefiable and non-liquefiable sands. Furthermore, per the investigation of Asadi (2022), ε_{ay} is less sensitive to the relative density and confining pressure of soils, and it is significantly dependent on the material type. The original definition of ε_{ay} has been modified by Asadi et al. (2022) to take into account the observation that the *CRR* of soils has an inverse relation with σ'_c (i.e., $CRR \propto \frac{1}{\sigma'_c}$); the modified cyclic yield strain is re-defined as:

$$\varepsilon_{ay,m} = \frac{CRR \times \sigma'_c}{G_{\max}} \qquad (1)$$

The investigated values of $\varepsilon_{ay,m}$ for reconstituted NP and Toyoura sands are illustrated in Fig. 8 versus their PC. It is evident from the graph that the magnitude of $\varepsilon_{ay,m}$ is significantly influenced by the PC of the NP sands, i.e., as the PC increases, the $\varepsilon_{ay,m}$ also increases. Furthermore, the results for Toyoura sand as well as those for the ordinary Japanese sands that were investigated by Amoly et al. (2016) are also illustrated in the figure. It can be seen that NP sands have higher $\varepsilon_{ay,m}$ when compared with ordinary sands due to the existence of crushable pumice sand particles in their soil matrix, resulting in their lower $G_{\max}$ and higher CRR, as mentioned earlier.

Since $\varepsilon_{ay,m}$ relates CRR to $G_{\max}$ ($=\rho V_s^2$, where ρ is the bulk density of soils) and is only material-dependent, it can be used as a constant strain parameter to establish simplified $CRR - V_s$ relations for liquefaction assessment of sands. More importantly, the $\varepsilon_{ay,m}$ is highly dependent on the PC of NP sands and, therefore, the effect of PC can be incorporated in the liquefaction assessment of NP sands.
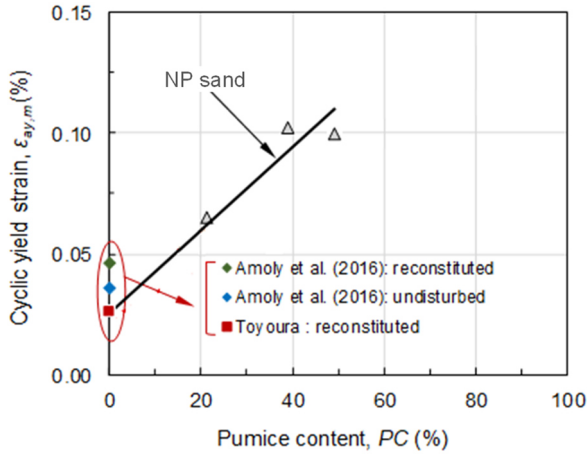

Figure 8. Relationship between cyclic yield strain, $\varepsilon_{ay,m}$, and pumice content, PC, for the tested sands.

4. *CRR-V$_s$* correlation

4.1. Conversion to field conditions

In order to establish the $CRR - V_s$ correlation for NP sands considering field conditions, the measured laboratory values of V_s and CRR are first converted into field condition, denoted as V_{s1} and $CRR_{(Field)}$, respectively, using the following procedure:

$$V_{s\,(Field)} = V_{s\,(Laboratory)} \left(\frac{1 + 2K_0}{3}\right)^{-n} \qquad (2)$$

where K_0 is the lateral earth pressure coefficient under field condition and n is the power coefficient of confining pressure (Robertson et al. 1995). Then, the V_{s1} is obtained by normalising the $V_{s(Field)}$ values with respect to the reference overburden stress ($P_a =100$ kPa) using Eq. 3 (Andrus and Stokoe 2000).

$$V_{s1} = V_{s\,(Field)} \left(\frac{P_a}{\sigma'_v}\right)^n \qquad (3)$$

where σ'_v is the effective overburden pressure. Note that the values of n in the above equations can be defined from Fig. 4 using $n=m/2$ for the appropriate specimen.

Next, the Seed (1979) conversion method, shown in Eq. 4, is followed to convert the obtained CRR values from triaxial testing into field conditions:

$$CRR_{Field} = \left(\frac{1+2K_0}{3}\right) r_c \, CRR_{(Laboratory)} \qquad (4)$$

where r_c is a constant value that takes into account the multi-directional shaking effects in the field, with values of 0.9-1.0 (Rauch et al. 2000). For normally consolidated soils, $K_0 \approx 0.5$, while Pender et al. (2006) reported a lower $K_0 \approx 0.4$ for pumice-rich sands due to their irregular surface texture and low unit weight. Therefore, in this study, $K_0=0.4$ is considered for NP sands in the above conversion, while $K_0=0.5$ is used for Toyoura sand. Taking $r_c =0.95$, the liquefaction resistance of soils under field conditions would be about 57% of their CRR values from triaxial testing (i.e. $CRR_{(Field)} = 0.57\, CRR_{(Laboratory)}$).

By substituting Eqs. 3 and 4 into the cyclic yield strain equation (i.e., Eq. 1), the $\varepsilon_{ay,m}$ value could also be converted into field conditions as follows:

$$\varepsilon_{ay,m(Field)} = r_c \left(\frac{1 + 2K_0}{3}\right)^{2n+1} \left(\frac{\sigma'_v}{P_a}\right)^{2n} \varepsilon_{ay,m} \qquad (5)$$

With the further substitution of the equation $G_{\max} =\rho V_s^2$ into Eqs. 1 and 5, it is possible to develop the $CRR_{(Field)} - V_{s1}$ relation using the $\varepsilon_{ay,m(Field)}$ values for NP sands. The $CRR_{(Field)} - V_{s1}$ relation is developed using the cyclic yield strain parameter as in Eq. 6.

$$CRR_{Field} = \frac{3\rho}{(1 + 2K_0)\, \sigma'_v} \varepsilon_{ay,m(Field)} V_{s1}^2 \qquad (6)$$

4.2. *CRR$_{field}$ – V$_{s1}$* correlations

Using Eq. 6, the correlation curves for the NP sands as well as for Toyoura sand are plotted in the $CRR_{Field} - V_{s1}$ chart shown in Fig. 9. Also plotted in the figure are the curves that are available in the literature for ordinary sands (e.g., Andrus and Stokoe 2000; Kayen et al. 2013). The data points shown in the figure are those obtained from the laboratory tests but converted into field conditions. Note that the n-values used in the above equations (for field conversions) are found from Fig. 4(a), i.e., $n=0.36$ and 0.37 for NP3 and NP4 sands, respectively, while NP1 sand has $n==0.3$ and Toyoura sand has $n=0.25$.

It is evident from the chart that the developed empirical correlations using Eq. 6 for: (1) NP3 and NP4 sands, with $\varepsilon_{ay,m} \approx 0.1\%$ and $PC \approx 40$-50%; (2) NP1 sand, with $\varepsilon_{ay,m} \approx 0.065\%$ and $PC \approx 20\%$; and (3) Toyoura sand, with $\varepsilon_{ay,m} \approx 0.02\%$, correlate well with the data points obtained from laboratory testing. As seen in Fig. 9, the curve for Toyoura sand plots in a similar region as those for ordinary sands, almost mimicking the plot of Kayen et al. (2013). On the other hand, the curves for NP3 and NP4 sands plot significantly far to the left of these curves, indicating that the $CRR_{(Field)} - V_{s1}$ curves for ordinary
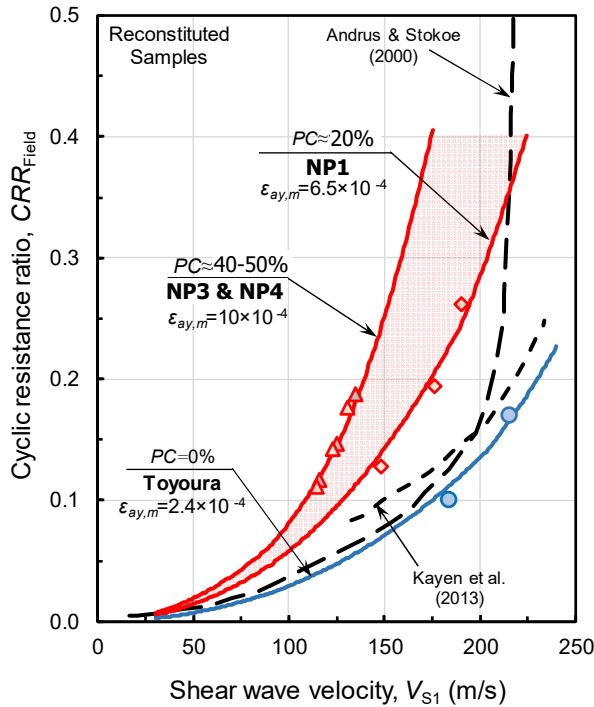
Figure 9. $CRR_{(Field)} - V_{s1}$ chart for NP sands, compared with ordinary sands (including Toyoura sand).

sands would significantly underestimate the liquefaction resistance of the NP materials for the same V_{s1} values. This is consistent with the observations made by Orense et al. (2020) that current empirical methods developed for ordinary (hard-grained) sands would underestimate the liquefaction resistance of pumice-rich sands. Furthermore, the curve for NP1 sand plots between the curve for NP3/NP4 sands and that for ordinary sands. This implies that the number of crushable pumice particles present in the soil matrix, expressed in terms of pumice content (PC), has an important effect on the observed correlations.

5. Concluding remarks

Based on the results obtained in this study, the following conclusions can be drawn:

- Reconstituted NP sands had significantly lower G_{max} when compared to ordinary sands (e.g., Toyoura sand) due to the presence of porous and crushable pumice particles within their soil matrix. Such vesicular and lightweight pumice particles in the NP sand matrix led to their lower shear wave velocity and lower bulk unit weight. Furthermore, the NP specimens that were characterised as high pumice content materials have lower G_{max} values compared to the low pumice content samples.
- The presence of pumice sand components in the NP sands also resulted in their higher deformability/ compressibility during the cyclic testing when compared with Toyoura sands. Such high deformability contributed to their higher contractive tendency, resulting in a substantial increase in excess pore water pressure (EPWP).
- NP sands had substantially higher values of cyclic yield strain ($\varepsilon_{ay,m} \propto CRR/G_{max}$) when compared to ordinary sands. Furthermore, NP sands with higher

pumice contents had higher $\varepsilon_{ay,m}$ values than those with lower PC. This would indicate the significant effect of the pumice sand components on the cyclic behaviour of NP sands.

- The $CRR_{(Field)} - V_{s1}$ correlations for liquefaction assessment of NP sands plotted further to the left side of the curve for ordinary sands as the PC increased. This showed that the current empirical relations for ordinary sands are not appropriate to use in estimating the liquefaction resistance of NP sands containing a significant amount of pumice sand grains.

Acknowledgements

References

Amoly, R. S., Ishihara, K., and Bilsel, H. 2016. "The relation between liquefaction resistance and shear wave velocity for new and old deposits." Soils Found, 56 (3): 506-519.

Andrus, R. D., and Stokoe, K. H. 2000. "Liquefaction resistance of soils from shear-wave velocity." J Geotech Geoenviron, 126 (11): 1015-1025.

Asadi, M. S., Asadi, M. B., Orense, R. P., and Pender, M. J. 2018. "Undrained cyclic behavior of reconstituted natural pumiceous sands." J Geotech Geoenviron, 144 (8): 04018045.

Asadi, M. S., Orense, R. P., Asadi, M. B., and Pender, M. J. 2019. "Maximum dry density test to quantify pumice content in natural soils." Soils Found, 59 (2): 532-543.

Asadi, M. B., Asadi, M. S., Orense, R. P., and Pender, M. J. 2020. "Small-strain stiffness of natural pumiceous sand." J Geotech Geoenviron, 146 (6): 06020006.

Asadi, M. B., Orense, R. P., Asadi, M. S., and Pender, M. J. 2022. "A unified approach to link small-strain shear modulus and liquefaction resistance of pumiceous sands." Soils Found, 62 (2022): 101098.

Kayen, R., Moss, R., Thompson, E., Seed, R., Cetin, K., Kiureghian, A. D., Tanaka, Y., and Tokimatsu, K. 2013. "Shear-wave velocity-based probabilistic and deterministic assessment of seismic soil liquefaction potential." J Geotech Geoenviron, 139 (3): 407-419.

Kokusho, T. 1980. "Cyclic triaxial test of dynamic soil properties for wide strain range. " Soils Found, 20 (2): 45–60.

Ladd, R. 1978. "Preparing test specimens using undercompaction." Geotech Test J, 1(1): 16-23.

Miura, S., Yagi, K., and Asonuma, T. 2003. "Deformation-strength evaluation of crushable volcanic soils by laboratory and in-situ testing." Soils Found, 43 (4): 47-57.

Orense, R. P., Pender, M. J., and O'Sullivan, A. 2012. "Liquefaction characteristics of pumice sands." Rep EQC 10/589. Auckland, New Zealand.

Orense, R. P., Asadi, M. B., Stringer, M. E., and Pender, M. J. 2020. "Evaluating liquefaction potential of pumiceous deposits through field testing: case study of the 1987

Edgecumbe earthquake." Bull NZ Soc Earthq Eng, 53 (2): 101-110.

Pender, M. J., Wesley, L. D., Larkin, T. J., and Pranjoto, S. 2006. "Geotechnical properties of a pumice sand." Soils Found, 46 (1): 69-81.

Rauch, A. F., Duffy, M., and Stokoe II, K. H. 2000. "Laboratory correlation of liquefaction resistance with shear wave velocity." Geotech Spec Publ, ASCE, 110: 66-80.

Robertson, P. K., Sasitharan, S., Cunning, J. C., and Sego, D. C. 1995. "Shear-wave velocity to evaluate in-situ state of Ottawa sand." J Geotech Eng, 121 (3): 262-273.

Sahaphol, T., and Miura, S. 2005. "Shear moduli of volcanic soils." Soil Dyn Earthq Eng, 25 (2): 157–165.

Seed, H. B. 1979. "Soil liquefaction and cyclic mobility evaluation for level ground during earthquakes." J Geotech Eng Div, 105 (2): 201-255.